THE ROLE OF MRI IN ASSESSMENT OF MYOCARDIAL VIABILITY

Essay submitted for partial fulfillment Of Master Degree in Radiodiagnosis Presented by

Yasser Mohammed Ali Ismail

M.B.B.CH

Under supervision of

Prof. Dr. Maha Hussein Anwar Abd ElSalam

Professor of Radiodiagnosis Faculty of medicine Ain Shams University

Dr. Hazem Fawzy Abou Elhamayed

Assistant Professor of Radiodiagnosis Faculty of medicine Ain Shams University

> Faculty of medicine Ain shams university 2011

دورأشعة الرنين المغناطيسي في تقييم حيوية عضلة القلب

بحث مقدم توطئه للحصول على درجة الماجستير في الأشعة التشخيصية مقدم مِن

ياسر محمد على اسماعيل

بكالوريوس الطب والجراحة

تحت إشرافِ الأستاذة الدّكتورةِ/ مها انور حسين

أستاذ الأشعة التشخيصية كليّة الطبّ جامعةً عين شمس

الدّكتور/حازم فوزى أبوالحمايّد

أستاذ مساعد الأشعة التشخيصية كليّة الطبّ جامعةً عين شمس

> كليّة الطبّ جامعة عين شمس ٢٠١2

LIST OF CONTENTS

	Page
1.	INTRODUCTION
2.	GROSS ANATOMY OF THE HEART1
3.	MRI ANATOMY OF THE HEART 14
4.	PATHOLOGY OF IHD29
5.	MRI MANIFESTATION OF IHD42
6.	SUMMARY & CONCLUSION103
7.	REFERENCES105
Q	ARARIC SIIMMARV

ACKNOWLEDGMENT

First and Foremost thanks to Allah, the Most Merciful and Gracious.

I wish to express my deepest appreciation and sincere gratitude to **Prof Dr.Maha Hussein Anwer**, Professor of Radiodiagnosis, Faculty of Medicine, Ain Shams University, for planning, supervising this study and for his valuable instructions and continuous help.

My deep gratitude to Dr. Dr. Hazem Fawzy
Assistant Professor of Radiodiagnosis Faculty
of medicine Ain Shams University, for her
support and help.

Also, I would like to express my gratitude and appreciation to my father, mother, lovely wife and my family who were supporting me all my life.

Yasser Mohammed Ali



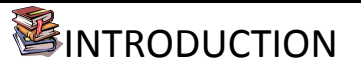
INTRODUCTION

Ischemic heart disease (IHD) is the most common symptomatic manifestation of cardiovascular disease and by far the leading cause of mortality. Atherosclerotic vascular disease is very common and most adults have some degree of atherosclerosis. The presence of risk factors such as hypertension, smoking, hypercholesterolemia, diabetes and obesity identifies a large proportion of patients who are at increased risk for developing symptomatic IHD (*Grainger et al, 2008*).

Cardiac magnetic resonance imaging (CMRI) is a rapidly developing new modality with applications in clinical cardiology for detection and assessment of myocardial ischemia and viability (Wagner et al, 2003).

CMRI has recently been applied successfully to the assessment of myocardial perfusion. CMRI has also been shown to assess accurately the extent of injury after a myocardial infarction and the presence of myocardial viability (*Theodoros et al, 2001*).

CMRI perfusion imaging has matured to a point where it can be routinely applied to assess patients with coronary artery disease and ischemic cardiomyopathy. The method has been compared to invasive, catheter-based as well as other noninvasive imaging modalities (echocardiography, single-photon emission computed tomography [SPECT], and positron emission tomography [PET]) for the evaluation of patients with coronary artery disease. Besides



qualitative evaluation of MR perfusion images, an absolute quantification of global, regional and transmural myocardial perfusion is possible. A relative or absolute myocardial perfusion reserve has been determined noninvasively with MR perfusion imaging, and can provide good agreement with the invasive assessment (*Muhling et al,2003*).

The use of magnetic resonance (MR) imaging for cardiac diagnosis is Expand ing, aided by the administration of paramagnetic contrast agents for a growing number of clinical applications (*Edelman et al*, 2004).

Cardiac MRI allows an accurate evaluation of myocardial morphology, function, perfusion, and tissue damage in a noninvasive way (*Belloni et al*, 2008).

Cine imaging is important in the evaluation of cardiac volumes and kinesis and is now considered the reference standard for the assessment of cardiac function and characterization of myocardial tissue abnormalities. (*Reichek et al.*, 2008).

Coronary arteries diseases can be obtained by computed tomography angiography (CTA), this requires significant radiation and iodinated intravascular contrast medium. CMR for these applications does not usually require contrast agent, and even when required, the risk is much less than that associated with iodinated contrast

INTRODUCTION

media. Direct comparison of the best MDCTA and coronary MRA shows that these techniques have essentially equivalent accuracy however MDCTA is a quicker study and is easier to use, and used in patient where MRI is absolutely contraindicated (such as prosthetic valve, pacemaker and stents(*Grainger et al*, 2008).

For these reasons, cardiac MRI has become an important diagnostic tool for IHD and is the new reference standard for the assessment of cardiac perfusion (*Belloni et al*, 2008).

LIST OF ABBREVIATIONS

AA Ascending Aorta

AMI Acute Myocardial Infarction

AO Aorta

APM Anterior Papillary MuscleATP Adenosine triphosphate

AV Aortic ValveAZV Azygos Vein

B-SSFP Balanced Steady State Free Precession

C Carina

CAD Coronary Artery disease

CE-IR MRI Contrast Enhanced Inversion Recovery MRI

CI Cardiac index

CMRI Cardiac Magnetic Resonance Imaging

CNR Contrast to Noise Ratio

CO Cardiac OutputCS Coronary sinus

CTA Computed Tomography Angiography

DAo Descending Aorta

DSMRI Dobutamine Stress MRI

ECF Extracellular FluidECG ElectrocardiogramEDV End Diastolic Volume

Es Esophagus

ESV End Systolic Volume ETL Echo Train Length

FAME Fast Acquisition with Multiple Excitation

FE Field EchoFFE Fast Field Echo

FID Free Induction Decay

FIESTA Fast Imaging Employing Steady-state

Acquisition

FISP Fast Imaging with Steady Precession

Gd-DTPA Gadolinium Diethyl Triaminic Pentaacetic Acid

GE Gradient Echo Heart Rate

IAS Inter-Atrial Septum
 IHD Ischemic Heart Disease
 IR Inversion Recovery
 IVC Inferior Vena Cava
 IVS Inter Ventricular Septum

IVS Inter-Ventricular Septum

LA Left Atrium

LAA Left Atrial AppendageLAD Left Anterior DescendingLCA Left Coronary Artery

LCC Left Coronary Sinus

LCCA Left Common Carotid Artery

LCX Left CircumflexLI Left InferiorLL Left Lung

LMB L
LMB L
Left Main Bronchus
LPA Left Pulmonary Artery
LSA Left Subclavian Artery

LV Left Ventricle

LVOT Left Ventricular Outflow Tract

MB Moderator Band

MDCT Multi-Detectors Computed TomographyMDCTA Multi-Detectors Computed Tomograph

Angiography

MI Myocardial Infarction

MPRi Myocardial Perfusion Reserve indexMRA Magnetic Resonance AngiographyMRI Magnetic Resonance Imaging

MV Mitral Valve

PA Pulmonary Artery

PDA Posterior Descending ArteryPET Positron Emission Tomography

PLB Posterior Left Branch

PPM Posterior Papillary Muscle

PV Pulmonary VeinsRA Right Atrium

RAA Right Atrial Appendage

RARE Rapid Acquisition with Relaxation Enhancement

RCA Right Coronary ArteryRCC Right Coronary Sinus

RCCA Right Common Carotid Artery

RFP Radio Frequency Pulse

RI Right Inferior

RMB Right Main stem BronchusRPA Right Pulmonary Artery

RS Right Superior

RSA Right Subclavian Artery

RV Right Ventricle

RVOT Right Ventricular Outflow Tract

SDC Sudden Cardiac Death

SE Spin Echo

SENSE Sensitivity Encoding SNR Signal to Noise Ratio

SPECT Single Photon Emission Computed Tomography

SPGR Spoiled Gradient-Recalled EchoSSFP Steady State Free Precession

SV Stroke Volume

SVC Superior Vena Cava

T Tesla

T2wSTIR T2Weighted Short-tau Inversion Recovery

TF Turbo Factor

TR Time of RepetitionTSE Turbo Spin EchoTV Tricuspid Valve

WMA Wall Movement Abnormality

2D Two Dimentional3D Three Dimentional

List of Figures

	Page No	<u> </u>
Fig.(1):	Sternocostal surface	 2
Fig. (2):	Base and diaphragmatic surface	
Fig. (3):	Right aterium	
Fig. (4):	Right ventricle	
Fig. (5):	Left ventricle	
Fig. (6):	Semilunar valve	9
Fig. (7):	Normal anatomy of coronary arteries	11
Fig. (8):	The origin of coronary arteries	12
Fig. (9):	Position of the heart in the thorax	14
Fig. (10):	Right atrium at end diastole and end systole Horizontal long-axis images using a balanced SSFP technique	
Fig. (11):	Left atrium at end diastole and end systole Horizontal long-axis images using a balanced SSFP technique	16
Fig. (12):	Right and left atrial appendage. Short-axis images using a 3D balanced-SSFP technique	
Fig. (13):	Atrial (inter-atrial) septum. Horizontal long-axis image using a balanced-SSFP technique	19
Fig. (14):	Moderator band. Horizontal long-axis view, using the balanced-SSFP technique	20
Fig. (15):	Components of the right ventricle. long-axis image	21
Fig. (16):	Gradual wall thinning towards the LV apex. Compared with the lateral LV wall segments at end systole and end diastole,	22
Fig. (17):	Components of the left ventricle.Left ventricular inflow outflow tract flow view at end diastol,	23

Fig. (18):	Left ventricular papillary muscles. Left ventricular outflow tract	23
Fig. (19):	Essential characteristics of the morphologically right and leftventricle	24
Fig. (20):	Mid ventricular short axis. Showing the convexity of the septum towards right ventricular cavity	25
Fig. (21):	Tricuspid and mitral valve. Shortaxis view through atrioventricular valves, using balanced-SSFP diastole	27
Fig (22):	Aortic valve cusps in closed and open condition y	27
Fig. (23):	Origin and proximal course of coronary arteries. Short-axis view through the aortic root.	28
Fig. (24):	Typical Progression of Coronary Atherosclerosis	32
Fig. (25):	Effects of ischemia and reperfusion on myocardial tissue after proximal coronary artery occlusion	37
Fig. (26):	Comparison of retrospective cine MRI (left) and real-time ungated cine MRI (right) 45	
Fig. (27):	Prospective triggering . In this example of a multiphase acquisition, after eachR-wave,	46
Fig. (28):	Technical modalities of MRI and their applications in cardiovascular studies	47
Fig. (29):	Spin-echo T1 w image in a transverse plane showing the characteristic signal absence of moving blood in the cardiac chambers and vessels, as well as the high signal intensity generated by fat tissue. Myocardium	49
Fig. (30):	Multiphase GE sequence. Twelve frames showing different phases of the cardiac cycle in a left ventricular horizontal long-axis view (4 chambers)	50

Fig. (31):	SSFP sequence on a longitudinal vertical plane of the left ventricle showing a signal void	50
Fig. (32):	Balanced steady-state free precession (b-SSFP) cine MR image in cardiac short axis. In comparison with standard gradient-echo cineMRI	52
Fig. (33):	Comparison of spin-echo acquisition with gradient reversal acquisition. (a) Midsystolic spin-echo MR image(b) Gradient reversal MR image	52
Fig. (34):	: End-diastolic (left) and end-systolic (right b- SSFP cine MR image in horizontal long-axis orientation	
Fig. (35):	CE-IR MRI, cardiac short—axis (left) and vertical long—axis	54
Fig. (36):	Ascending aorta velocity encoded MR imaging. Axial plan at the level of great vessel	
Fig. (37):	Gradient-echo coronary MR angiography image of the left anterior descending (LAD) coronary artery	57
Fig. (38):	Cardiac axis imaging planes for the left ventricle; images acquired using a balanced steady-state free precession sequence	59
Fig. (39):	Transverse images	60
Fig. (40):	Coronal images	61
Fig. (41):	Sagittal images	62
Fig. (42):	Short-axis images	63
Fig. (43):	Horizontal long-axis images	64
Fig. (44):	Vertical long-axis images	65
Fig. (45):	Axial plane showing the artifact produced by the suture wire	66
Fig. (46):	Diagram of vertical long-axis (VLA), horizontal long-axis (HLA), and short-axis (SA) planes	68
	1~==, p	

Fig. (47):	circumferential polar plot, of the 17 myocardial segments	68
Fig. (48):	Subsequent division of SA slices into 6 basal, 6 mid-cavity, and 4 apical segments, with segment 17 being the apex seen on the long-axis views	69
Fig. (49):	Assignment of the 17 myocardial segments to the territories of (LAD), (RCA), and (LCX).	70
Fig. (50):	balanced-SSFP technique. (a) Vertical long- axis (b) midventricular short-axis,	74
Fig. (51):	Advantages of b-SSFP in evaluation of ventricular function BSA, body surface area;	75
Fig. (52):	Example of complete short-axis dataset in b-SSFP. End-diastolic (left) and end systolic (right) frames	76
Fig. (53):	Example of a short-axis MR C-spatial modulation of magnetization (SPAMM) myocardial tagging study	78
Fig. (54):	Practical schematic for dobutamine-stress MRI (DSMRI)	81
Fig. (55):	Qualitative assessment of myocardial first- pass perfusion. Example of a large anterior perfusion defect	86
Fig. (56):	For generating signal intensity—time curves, first the endo- and epicardial contours of the myocardium have to be drawn and corrected in each image for shift and motion	87
Fig. (57):	Short axis CE-IR MR images in a patient with a large transmural inferior wall infarction	88
Fig. (58):	a Schematic of the contrast kinetics in different pathophysiological states after myocardial infarction.	89
Fig. (59):	The duration of ischemia is a major determinant of infarct size and the transmural extent of infarction	89

Fig. (60):	The appearance of a normal heart and two inferior myocardial infarctions. An inversion recovery delayed-enhancement image	90
Fig. (61):	Subendocardial myocardial infarction CE-IR MR images in short-axis	91
Fig. (62):	Transmural myocardial infarction	92
Fig. (63):	Transmural myocardial infarction with microvascular obstruction. Short-axis CE-IR MR images	93
Fig. (64):	Occlusive myocardial infarction in the acute to subacute phase (day 5). a CE-IR MR shortaxis images taken within 2 min after contrast administration	95
Fig. (65):	Complications after myocardial infarction I. Chronic complicated myocardial infarction is illustrated with CE-IR MR images in short- axis	98
Fig. (66):	Appearance of left ventricular thrombus associated with an acute anterior and apical myocardial infarction.	98
Fig. (67):	Whole heart coronary MR angiography acquired with a free breathing, steady state free precession sequence	100
Fig. (68):	Whole heart coronary MR angiography in a patient with anomalous right coronary artery. Curved multiplanar reformatted MR angiographic image	100
Fig. (69):	Coronary CT angiography (64-slice CT) and whole heart coronary MR angiography	
Fig. (70):	. 31P spectra from the septal myocardium three weeks after acute MI	102